Accepted Manuscript

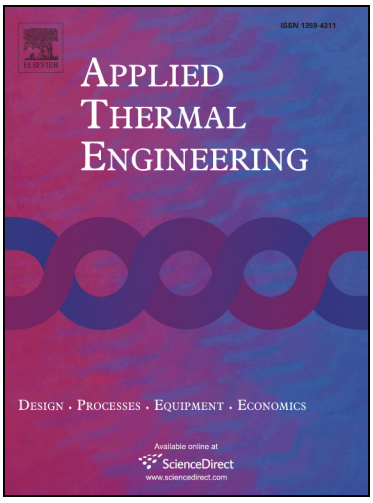


# Charging performance of a $CO_2$ semi-clathrate hydrate based PCM in a lab-scale cold storage system

Xiaolin Wang, Mike Dennis

PII: S1359-4311(17)30821-9
DOI: http://dx.doi.org/10.1016/j.applthermaleng.2017.07.201
Reference: ATE 10869

To appear in: *Applied Thermal Engineering*

Received Date: 7 February 2017
Revised Date: 17 July 2017
Accepted Date: 31 July 2017

Please cite this article as: X. Wang, M. Dennis, Charging performance of a $CO_2$ semi-clathrate hydrate based PCM in a lab-scale cold storage system, *Applied Thermal Engineering* (2017), doi: http://dx.doi.org/10.1016/j.applthermaleng.2017.07.201

This is a PDF file of an unedited manuscript that has been accepted for publication. As a service to our customers we are providing this early version of the manuscript. The manuscript will undergo copyediting, typesetting, and review of the resulting proof before it is published in its final form. Please note that during the production process errors may be discovered which could affect the content, and all legal disclaimers that apply to the journal pertain.

ACCEPTED MANUSCRIPT

# Charging performance of a $CO_2$ semi-clathrate hydrate based PCM in a lab-scale cold storage system

Xiaolin Wang*, Mike Dennis

*Research School of Engineering, the Australian National University, Canberra 2601, Australia*

**Abstract:** Cold thermal energy storage aids in the efficient deployment of thermal energy whenever there is a mismatch between energy generation and energy use. In this study, a lab-scale demonstration of cold storage system was built to investigate the performance of $CO_2$ semi-clathrate hydrate as a cold storage material in the charge of a realistic cold thermal storage. The experimental rig was basically a vessel equipped with an external loop and an ultrasonic crystallizer to boost the hydrate formation. The hydrate was formed from a salt solution composed of tetra-n-butyl ammonium bromide 20 wt%, tetra-n-butyl ammonium fluoride 0.25 wt% and sodium decyl sulfate 0.15 wt%. At a constant pressure condition of 5.0 bar, the hydrate formation was triggered by the heat transfer fluid at $7.5^0$C. The charged cooling capacity of two control strategies, namely 'constant pressure' and 'constant mass', were compared. The repeatability and stability of hydrate formation conditions were studied. It was indicated that $CO_2$ semi-clathrate hydrate could serve in cold storage systems effectively. However, it was also found that under the experimental conditions, hydrate formation was hard to thoroughly complete due to the lack of sufficient driving force or heat/mass transfer.

**Key words:** *$CO_2$ hydrates, cold thermal energy storage, charging temperature, charging rate, charged cooling capacity*

## 1 Introduction

The use of air conditioning is one of the main reasons for electrical power demand peaks during summer, accounting for as much as half of the power demands during the hot midday hours in some areas when electricity is most expensive [1]. At night, since utilities have spare electrical generating capacity after the demand falls, the wholesale electricity price is lowered as an incentive for consumption. It is therefore financially attractive to operate an electric air conditioning chiller at off-peak times. However, this strategy requires the chillers to shut down during peak-load hours and to have a backup system to provide cooling at those times.

**Xiaolin Wang**: PhD candidate, the Australian National University, xiaolin.wang@anu.edu.au

ACCEPTED MANUSCRIPT

Cold thermal energy storage (CTES) can be a backup to such systems. It refers to storage approaches that conserve cooling capacity by extracting heat from a storage medium, such as chilled water, ice and phase change materials (PCMs). It has become one of the primary means of addressing the electrical power imbalance between daytime demand and night-time abundance by providing cooling capacity during the day and using electricity at night. CTES can also serve in a solar cooling system to store extra cooling capacity and supply cooling in solar outage.

Latent heat CTES is believed to be advantageous among energy storage strategies due to the large storage capacity available in phase transition. PCMs and their applications in air conditioning systems have been widely studied in the last decade. Real et al. [2] explored an HVAC system with two PCMs thermal storage tanks - a cold tank used to make use of the low ambient temperatures at night to cool the PCM with a high chiller coefficient of performance (COP); and a second tank working as an alternative hot reservoir. It was found that the PCM tanks allowed the COP to be independent of the ambient temperature and an energy saving of 18.97% was obtained. In the work of Cheng et al. [3], a packed bed cold storage employing a fatty acid based composite PCM was designed for high temperature solar cooling application. A total of 450 spherical PCM capsules are randomly packed in the cylindrical segment, which has an inner diameter of 0.19m and an effective length 0f 0.84 m. Results showed that the charging rate and charged cooling capacity more depended on the heat transfer fluid (HTF) temperature, but the energetic efficiency less depended on it. With the chilled water at a flow rate of 100 $L \cdot h^{-1}$, the maximal accumulated cold stored was 1800 kJ. Castell et al. [4] presented an experimental study on a cold storage tank using a non-gelled hydrated salt mixture as PCM. It had a melting point of 27°C and a latent energy of 145 $kJ \cdot kg^{-1}$. It was also found that the system heat exchange effectiveness increased with decreasing flow rate and increasing heat transfer area. Zauner et al. [5] built a storage tank with 170 kg of high density polyethylene and a total mass of 600 kg based on a fin-tube heat exchanger. Its energy capacity, power characteristics and temperature profiles were studied in a thermal oil test rig. It was found that the stored energy for different operating temperatures and a mass flow of 1 $kg \cdot s^{-1}$ could be up to 27 kWh. In the work of Falco et al. [6], a storage tank was added in a traditional chiller-fan coil system to shave the electricity peak loads. The storage tank, made by a biphasic liquid packed inside and a water–water heat exchanger in the PCM volume, allowed direct-contact heat transfer between PCM and water. High efficiency was demonstrated in the charge – the storage tank could be completely charged in 54 min if the charging power was 5.7 kW. Besides, it was possible to recover 13–16% of the electricity in a small office which required a cooling power of 40 kW by implementing a scaled-up device of about 30 kWh. An experimental investigation on the operating characteristics of cold storage ejector

ACCEPTED MANUSCRIPT

cooling system with finned tube inside a cylindrical PCM tank was reported by Chen et al. [7]. The cold storage was placed in parallel with the evaporator. It could store the excess cooling capacity that the ejector produced and supply cooling when the ejector did not work. The performance parameters, such as the tank temperature, inlet and outlet HTF temperature, cold storage rate and capacity were measured at various mass flow rates at an evaporator temperature of 3–5$^0$C. The results demonstrated that the PCM cold storage integrated with ejector could help to maintain a more stable COP for the ejector cooling system. A new organic PCM with the freezing point of 7$^0$C and latent heat of 173.5 kJ· kg$^{-1}$ was proposed by Li et al. [8] for the use in a conventional cooling system using direct contact CTES tank. Simulations and experimental investigations on the charging process of the tank were presented. Influencing factors of HTF inlet temperature, flow rate of liquid PCM, charging time, cold storage capacity, and temperature distribution in the direct contact cold storage device were investigated. Comodi et al. [9] studied the feasibility of using CTES for building demand management in hot climate. A CTES was coupled to the existing cooling system in an office building in Singapore to address the opportunity to improve overall energy efficiency, exploiting the spread between peak and off-peak tariffs. Results indicated that it was possible to enhance the efficiency of the cooling system, achieving both energy and economic savings. The payback periods of different solutions ranged from 8.9 years to 16 years. In a study of Allouche et al. [10], an analysis of sensible and latent storage using water and the microencapsulated PCM was performed. The experiments were carried out in a 100 L horizontal cold storage equipped with two tube bundle heat exchangers in the top for the charge, and two similar ones in the bottom to ensure the discharge. The results showed that the amount of energy stored using the microencapsulated PCM was 53% higher than for water after 10 h of charging, for the same storage tank volume. A cold storage air conditioning system using tetra-n-butyl ammonium bromide (TBAB) clathrate hydrate slurry (CHS) as cold storage medium was built to study the CHS generation methods by Shi et al. [11]. The methods included continuously cooling, turning off refrigerator while crystals appeared, supercooling release and addition of CHS into supercooled TBAB aqueous solution. Results showed that both the second and fourth methods could better maintain the heat exchanger temperature, leading to higher COP. In addition, accession of TBAB CHS into TBAB supercooled solution could shorten the time of supercooling, resulting in about 21.8–35.4% shorter generation time. It was also found that higher flow rate resulted in higher COP.

Clathrate hydrates are crystalline solid compounds formed from water and gas molecules. Gas molecules (guest) are trapped in cages (host) that are composed of hydrogen-bounded water molecules. $CO_2$ molecules can form clathrate structure. The hydrate has a critical temperature of

ACCEPTED MANUSCRIPT

283.0 K and a critical pressure of 4.5 MPa [12]. $CO_2$ hydrates can offer a large phase change latent heat that leads to size and weight advantages. By using DTA Laurence et al. [13] deduced that the total dissociation enthalpy of the solid formed from the $CO_2$–water mixture was 507 $kJ \cdot kg^{-1}$(water). Thus $CO_2$ hydrate appears to have obvious advantages over many other types of PCM. It was also reported that when the global $CO_2$ mole fraction was 2.88 mol% and the temperature was 276.2 K, the hydrate fraction in the slurry was 2.8 vol% and the available enthalpy was up to $1.15 \times 10^4$ $kJ \cdot m^{-3}$(water) [14]. $CO_2$ hydrate also has suitable phase change temperatures in the range of 5–12$^0$C, which suits the characteristics of conventional air conditioning systems. Moreover, it is safe, non-toxic and non-flammable. Therefore, $CO_2$ semi-clathrate hydrate is considered as a promising cold storage material.

In the work of Zhou et al. [15], a model has been proposed for the prediction of $CO_2$ hydrate crystals production rate in fluidized bed heat exchangers. The system contained a fluidized bed $CO_2$ hydrate generator and a $CO_2$ hydrate slurry cold storage vessel, during the five hottest days of the reference climate data of Netherlands. The COP of the system composed of fluidized bed for hydrate generation and CTES appeared to be 23–43% higher than the COP of a conventional system. During the experiments with continuous removal of hydrate slurry, a solid concentration up to 35% was maintained. During the experiment in which only the originally injected $CO_2$ was consumed, a solid concentration up to 45% has been realized. An independent energy system for houses in cold regions was developed by Obara et al. [16] using a small-scale natural gas cogeneration, air-source heat pump, heat storage tank, and gas hydrate battery (GHB). To increase the formation speed of $CO_2$ hydrates, a ferrous oxide-graphite system catalyst was used. The ambient air of cold regions was used as a heat source for the formation process of the GHB, and the heat supplied by a geothermal heat exchanger was used for the dissociation process. Using a geothermal heat source, fuel consumption was halved due to an increased capacity for hydrate formation in the GHB, a shortened charging and discharging cycle, and a decrease in the freeze rate of hydrate formation space.

From previous studies, CTES systems using $CO_2$ hydrate as the PCM are associated with several problems including:

1. Supercooling may take place, which makes the required chilled water temperature lower to trigger hydrate formation. This reduces the chiller efficiency;
2. The induction delay in the hydrate formation makes it longer to initiate and complete the charging process;
3. The means of pressure control of the storage system may be challenging;

ACCEPTED MANUSCRIPT

4. The mass and heat transfer in the heat exchanger may cause agglomeration of the hydrate;
5. The operation cannot be completely reversed due to the low repeatability of hydrate formation.

In this study, a lab-scale experimental system was built to study the charging performance of a lab-scale demonstration of CTES system using a self-developed $CO_2$ hydrate based PCM. This material is composed of the $CO_2$–water system, TBAB salt and secondary prompters (surfactant and/or nanoparticle). The morphology of crystals during the charge is presented. Different modes of charging operation are conducted and the maximum valid chilled water temperature is sought using a stepwise method. Influencing factors of the charging rate, namely the chiller's set-point, the external flow rate and the ultrasonic vibration, are investigated. Two charge control strategies – 'constant mass' and 'constant pressure' of $CO_2$ are both tested. Besides, the $CO_2$ hydrate formation was repeated for 20 times to study the reversibility and repeatability of this PCM.

## 2 System configurations

The lab-scale demonstration system of the $CO_2$ semi-clathrate hydrate based CTES system is shown in Figure 1. The system is mainly composed of a storage vessel, a crystallizer and a thermostatic bath. Helical coils are located in the vessel and connected to the thermostatic bath; thus the temperature controlled water from the bath provides a cold and heat source to the CTES. The hydrate formation, storage and dissociation all take place within the vessel but outside the helical coils. The crystallizer is used to test the effect of ultrasonic vibration on the hydrate formation.

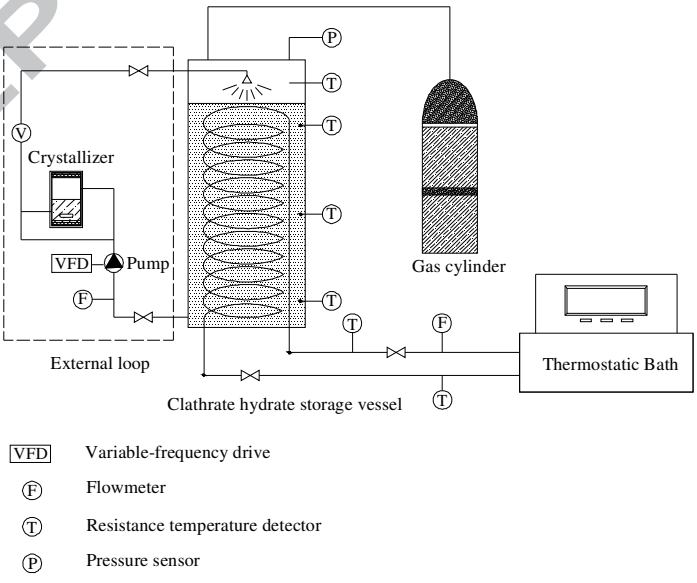


Figure 1 Schematic diagram of the lab-scale $CO_2$ hydrate cold storage system

ACCEPTED MANUSCRIPT

The appearance of the $CO_2$ hydrate storage vessel is shown in Figures 2. The vessel is an internal melt ice-on-coil system. Chilled water i used as the heat transfer fluid in a closed loop in the vessel. Chilled water is circulated through helical coils in the vertical part of the vessel and heat exchange is between the chilled water and the PCM outside the coils. The vessel is pressurized by $CO_2$ gas. In the horizontal part, pistons on both ends are used to adjust the inner volume of the vessel. The horizontal part has a diameter of 0.14 m and a length of 0.76 m; the vertical part has a diameter of 0.14 m and a length of 0.41 m. In this way, the inner volume can be changed from 8.6 to 16.5 L. The vessel is well insulated with glass wool to minimize heat loss from the outer surfaces.

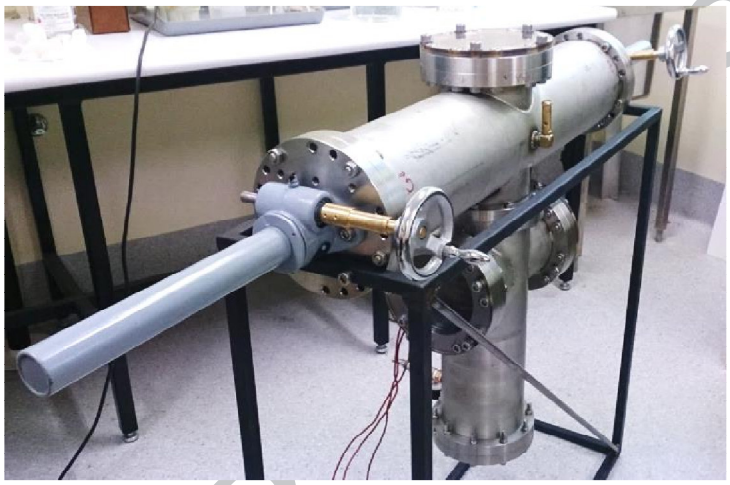

Figure 2 Appearance of the cold storage vessel

There are four platinum temperature sensors on the vessel wall (respectively 80, 180, 280 and 380 mm from the bottom) and two platinum temperature sensors in the inlet and outlet helical coils of the chilled water. All the sensors have been calibrated. The uncertainty of temperature measurement is $\pm 0.1^0$C and that of pressure measurement is ±0.05 bar.

There are a coolant loop and a hydrate slurry loop in the system. In the coolant loop, chilled water from the thermostatic bath flows in the helical coils to trigger the formation of $CO_2$ semi-clathrate hydrate outside of the coils. The flow rate of the chilled water is 3.6 $L \cdot min^{-1}$. In the slurry loop, the liquid AFS solution containing dissolved $CO_2$ gas and tiny formed hydrate particles in the vertical part are circulated from the bottom of the vessel to the crystallizer, and then pumped back to the top of the vessel (filled with $CO_2$ gas) through a nozzle. Rather than forming hydrate in a quiescent state, the slurry loop can prompt the hydrate formation by enhancing the contact between $CO_2$ gas and the water solution.

ACCEPTED MANUSCRIPT

For ice storage, the secondary coolant is usually ethylene glycol. It requires the chiller capable of producing charging temperatures in the range from –6 to –3$^0$C. In the discharge, ice storage provides sustained discharging temperatures of 2–3$^0$C. This temperature is too low for conventional space cooling, thus it is usually adjusted by mixing with return water. For the $CO_2$ hydrate based CTES system in the present work, the secondary coolant is water, which is typically required to provide a temperature of 7$^0$C for charging and 12$^0$C for discharging the cold store. The charging temperature is the normal design chilled water temperature for conventional air conditioning systems or air conditioning systems with water storage; thus it would result in minimal extra operating cost for operating the chiller with CTES.

The crystallizer is made of brass with an inner volume of 0.196 L. It has a slurry inlet, a slurry outlet and a gas inlet. Both ends are sealed with flanges and O-rings, and the side walls are transparent polycarbonate with white LEDs inlayed at the bottom for a clear view of the inside. A 50 W 40 kHz ultrasonic transducer is mounted on the side wall of the crystallizer, in close contact with the wall. The ultrasonic transducer is made to modulate its operating frequency between 19.08 and 41.66 kHz over a time cycle of several seconds. The side view and top view of the crystallizer with the ultrasonic transducer are shown in Figure 3. Both the cold storage vessel and the crystallizer can stand up to 10 bar.

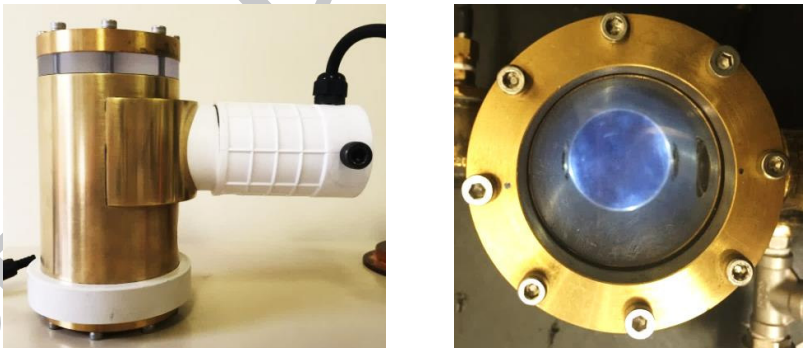

Figure 3 Appearance of the crystallizer of the cold storage system

## 3 Experimental procedures

At the start of the charging process, the pump is on and the solution is circulated in the external hydrate slurry loop. Pressure in the vessel is increased by injecting $CO_2$ gas from the gas cylinder (point I to point A in Figure 4). Once the design feed pressure is reached and the pressure is stable, the injection of $CO_2$ is stopped. Then the cooling is started by circulating the chilled water in the helical coils at a constant temperature that is lower than the formation temperature of the gas hydrate.

ACCEPTED MANUSCRIPT

During charging, three operation modes were conducted:

1. Storage vessel
2. Storage vessel + nozzle
3. Storage vessel + nozzle + crystallizer with ultrasonic vibration.

For the first mode, hydrate slurry loop is not put into use; for the second, the external slurry loop is used while the crystallizer does not work; for the third, both the external loop and the crystallizer are active, and the ultrasonic transducer operates.

In Figure 4, the hydrate formation takes place when crossing the liquid water–hydrate–vapor ($L_w$-H-V) equilibrium curve. To the left of the curve the system is in liquid water and hydrate ($L_w$-H); to the right of the curve the system is in liquid water and vapor ($L_w$-V). Thus, $CO_2$ and water at point A forms hydrate at point B and C. With respect to the vessel, the operation mode of charge can be either 'constant mass' or 'constant pressure'. The former is implemented when the gas inlet valve is closed after the design pressure is reached and the system becomes a closed control volume (from A to B); the latter is conducted when the gas inlet valve remains open to the gas cylinder via a regulator thus the pressure of the system is kept constant (from A to C). We observe that to cross the phase equilibrium curve, the 'constant pressure' mode is conducted at a higher formation temperature, thus the required chilled water temperature to charge the CTES can be higher than that for the 'constant mass' mode.

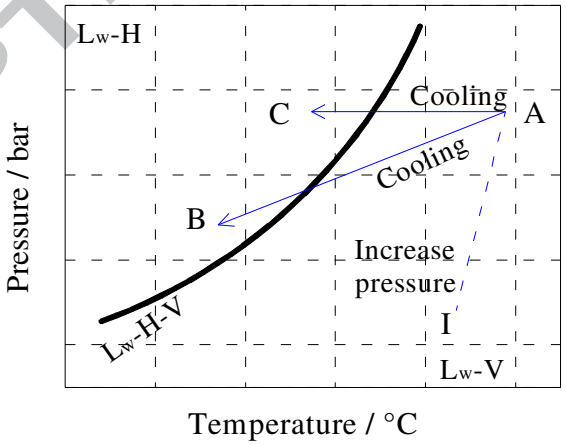


Figure 4 P-T correlation of hydrate formation under different operation modes in the charge

The control of formation pressure appears to offer a method to influence the freezing temperature of the hydrate. This feature allows the air conditioning system some flexibility in real time operation.

ACCEPTED MANUSCRIPT

For example, if dehumidification is not required, the chilled water temperature supplied by the CTES may be raised to say $12^0$C. Supply and discharge of energy over a tuneable range of temperatures is not offered by PCMs such as paraffins, eutectic salts or conventional ice.

## 4 System performance indicators

Generally, the performance indicators in the charge of internal melt PCM CTES systems are [17]:

- Charging temperature (including subcooling effect);
- Charging rate;
- Charged cooling capacity.

The designer can manipulate the chiller set point to control the rate of hydrate formation. This formation rate is determined by measuring the rate of heat added to the chilled water flow. However, a compromise must be made between hydrate formation rate and chiller efficiency. The aim is to fully charge CTES in the time available while minimizing chiller and auxiliary energy consumption.

The charging rate is calculated using the energy transfer associated with the bath water

$$Q_C = \dot{m}\, c_{p,HTF}(T_b - T_a) \tag{7.1}$$

where $\dot{m}$ is the mass flow rate of the bath water and $c_{p,HTF}$ is the specific heat of the bath water. $T_a$ and $T_b$ are the temperature of the inlet and outlet water temperature in the charging.

The charged capacity is calculated by integrating the instantaneous charging rate with respect to time. In this study, both the charging rate and charged cooling capacity will be assessed. Some influencing factors, such as chiller's set-point, external flow rate and ultrasonic vibration on the charging rate will be discussed.

## 5 Synergy of secondary promoters in hydrate formation

From a previous study on the effect of secondary promoters [18], for $CO_2$–TBAB hydrate the most favorable promoters are tetra-n-butyl ammonium fluoride (TBAF) at low mass fractions (0.1–0.5 wt%), sodium decyl sulfate (SDS) at low mass fractions (0.1–0.3 wt%) and $TiO_2$ nanoparticles in large size (80 nm). Within the mass fraction range/size, the promoters are blended in four cases, TBAF + SDS, TBAF + $TiO_2$, SDS + $TiO_2$ and TBAF + SDS + $TiO_2$, shown in Table 1, and the synergy of the combinations is tested. The formation is conducted at a feed pressure of 8.5 bar and a

ACCEPTED MANUSCRIPT

HTF temperature of 4.5$^0$C. During the test in a small-scale tube described in the previous study [18], the formation temperature, supercooling degree, induction time and $CO_2$ uptake are obtained from the temperature and pressure curve along the hydrate formation, and are shown in Figure 5.

Table 1 Combinations of secondary promoters at favorable concentrates/sizes

| Combination | Component |
|---|---|
| AFS | TBAB 20 wt% + TBAF 0.25 wt% + SDS 0.15 wt% |
| AFT | TBAB 20 wt% + TBAF 0.25 wt% + $TiO_2$ 80 nm |
| AST | TBAB 20 wt% + SDS 0.15 wt% + $TiO_2$ 80 nm |
| AFST | TBAB 20 wt% + TBAF 0.25 wt% + SDS 0.15 wt% + $TiO_2$ 80 nm |

All the formation temperatures are in a range of 6.5–7.5$^0$C, which is suitable for air conditioning chillers. The minimum supercooling degree is attained in the case of AFST at only 0.7$^0$C; some other combinations also achieve small extents of supercooling, namely 1.2$^0$C for AFS and 1.0$^0$C for AFT. The largest $CO_2$ uptake quantity is 0.349 g for AFS, followed by 0.348 g for AST. The induction time is short and useful for practical cold storage charge process for the case of AFS (26.3 min) and AFST (23.9 min). Overall, the best one among the candidates is AFS, which offers a large $CO_2$ uptake, a small supercooling degree and a short formation time. Therefore, the solution of AFS (TBAB 20 wt% + TBAF 0.25 wt% + SDS 0.15 wt%) is used in the $CO_2$ hydrate CTES system. The dissociation temperature of $CO_2$–AFS semi-clathrate hydrate was 10.4$^0$C with a difference between the freezing and melting temperature of 3.2$^0$C.

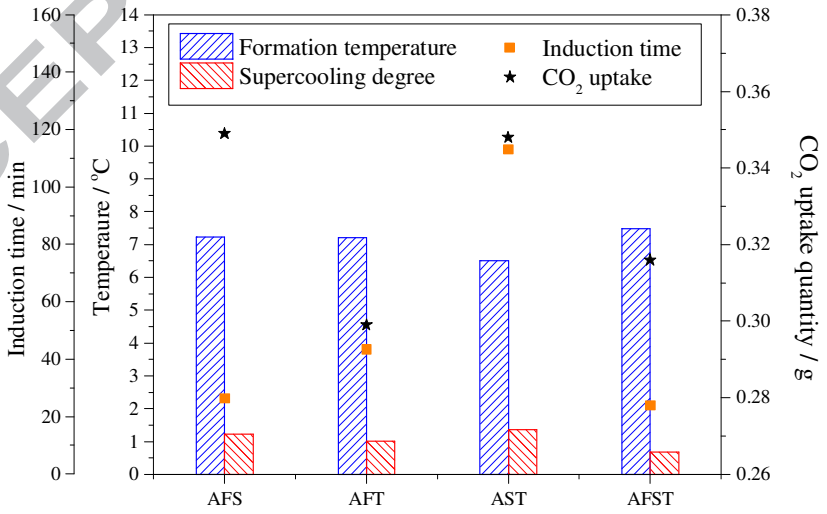


Figure 5 Formation behavior of different combinations of secondary promoters

ACCEPTED MANUSCRIPT

## 6 Morphology of charge

Photos of the inside of the vessel were taken during hydrate formation. The top and side photo before the experiment began is shown in Figure 6 (a) and (b), respectively.

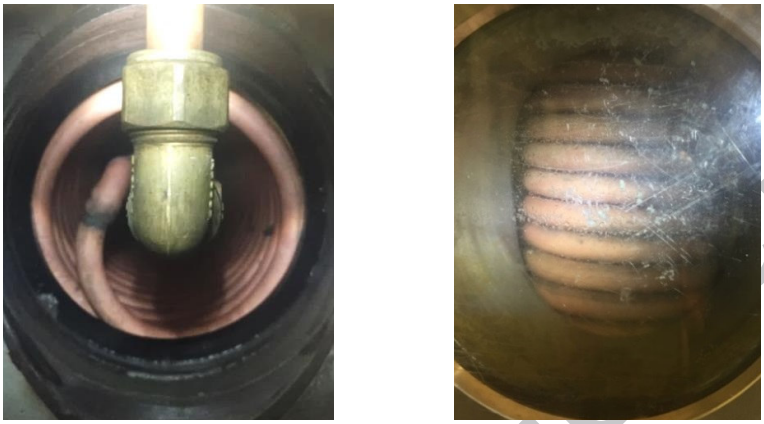

(a) Top view (b) Side view

Figure 6 Top and side view of the vessel before the hydrate formation

The first trial experiment was conducted using the 'constant mass' mode. The gas inlet was closed after the vessel's pressure became stable at 5.0 bar. The chilled water at a constant temperature of $7^0$C was circulated to the vessel. The external slurry loop was operating. At around 20 min after the start of cooling, a large pressure decrease was detected. A mass of foam of $CO_2$ and water mixture formed on the liquid surface, which could be viewed from the top window of the vessel (Figure 7). From the side windows, three layers were seen – on the top was the foam of $CO_2$ and water mixture, in the middle was the bulk of liquid and at the bottom was the formed hydrate solid piling up like snow (Figure 8). Foam was also seen from the top of the crystallizer, but this may have been circulated along with the liquid in the external slurry loop (Figure 9).

ACCEPTED MANUSCRIPT

Figure 7 Top view of the foam at the start of $CO_2$ hydrate formation

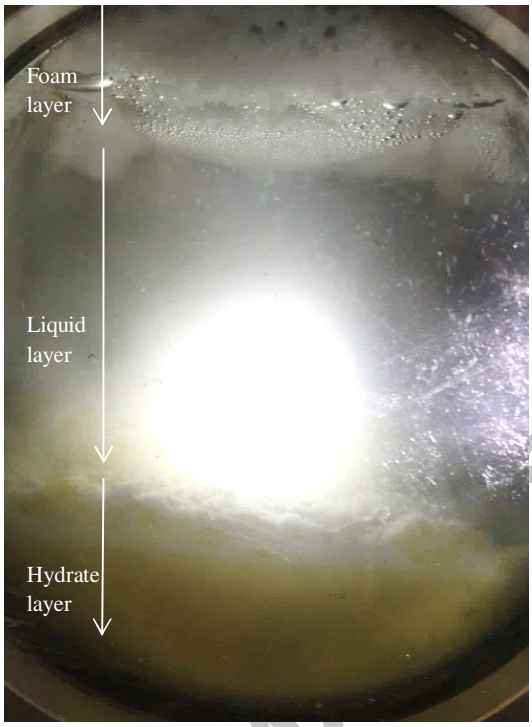


Figure 8 Side view of the layers during $CO_2$ hydrate formation

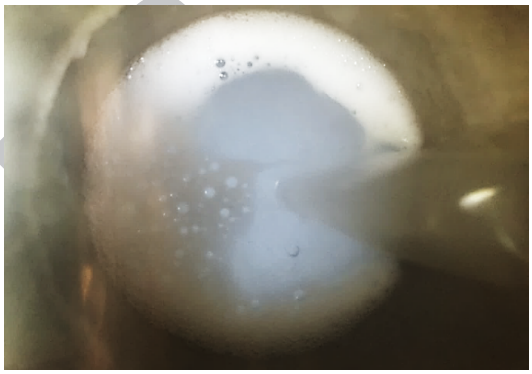

Figure 9 Top view of the crystallizer during $CO_2$ hydrate formation

At around 40 min after cooling, it became more obvious to see the small solid chips (hydrate particles) formed on the top of the liquid surface and sunk down to the bottom hydrate layer (Figure 10(a)). As the hydrate formation proceeded, the top foam layer became thicker and the formed hydrate gathered in large conglomerates. Gradually, large conglomerates of hydrate sunk down from the top, as shown in Figure 10(b). The bottom layer of hydrate became much thicker. The external surface of the coils also gained large adhesions of hydrate, due to the low coil temperature.

ACCEPTED MANUSCRIPT

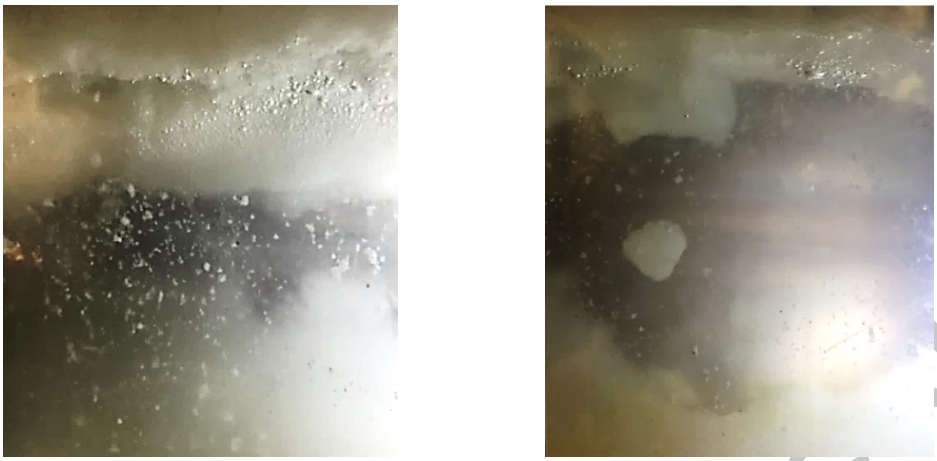

(a) Chippings (b) Solid chunks

Figure 10 Enlarged view of the dropping of formed $CO_2$ hydrate

When no further pressure drop was observed, the external pump was turned off and the chilled water was maintained at constant temperature. This was to avoid any blockage at the inlet of the pump as the solid fraction in the solution increased greatly. The formation of the hydrate became very slow due to the low mass transfer of $CO_2$ gas and because the heat transfer between the chilled water and the bulk hydrate was reduced by the thermal resistance of the already formed hydrate on the outer surface of the coils. The formation finally stopped because of the low overpressure driving force (the pressure decreased as the formation proceeded). Finally, the foam on the top became thick and mushy due to the increased fraction of solid hydrate (Figure 11).

Figure 11 Top view at the end of $CO_2$ hydrate formation

ACCEPTED MANUSCRIPT

For the purposes of observation, the remaining liquid was drained from the vessel and the coils emerged, as can be seen in Figure 12. The agglomeration of solid hydrate was visible on the surface of coils, and piled hydrate was at the bottom. The appearance the formed $CO_2$ semi-clathrate hydrate was just like ice.

Figure 12 Top view at the end of $CO_2$ hydrate formation after draining remained water solution

## 7 Results and discussions

### 7.1 Different operation modes of charging

This test (constant mass) was to study the effectiveness of charging the cold storage vessel in three operation modes – under static state, with the external loop (driven by the external pump), and with both the external loop and the ultrasonic vibration.

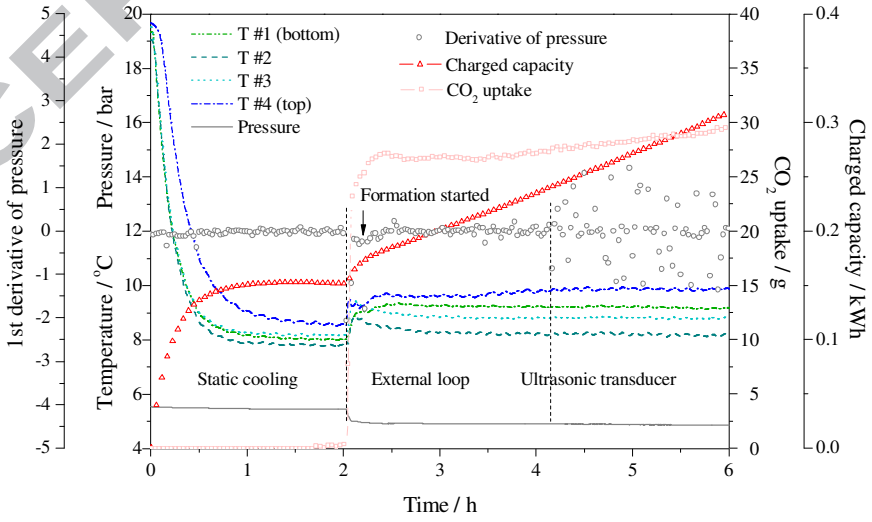


Figure 13 The charging process under different operation modes

ACCEPTED MANUSCRIPT

In the beginning, the vertical part of the vessel contained 6.5 L AFS solution and the horizontal part was filled with $CO_2$ gas. The initial pressure of the vessel was 5.5 bar and its temperature at 19.5$^0$C (the current room temperature). The variations of temperature, pressure, $CO_2$ gas uptake and charged capacity are shown in Figure 13. In the first stage (static cooling), chilled water at 7.0$^0$C was sent into the helical coils in the vessel to cool the solution. The pressure decreased with the temperature drop. The charged capacity first increased rapidly due to the large temperature difference for sensible heat transfer, and then it grew slowly. When the temperature curves became stable, the charged capacity was constant at 0.15 kWh.

During the static cooling process, no formed solid was visible; also, there was no peak observed in the temperature curve (temperature peak would indicate hydrate formation). Therefore, after 2.0 h in the second stage, the pump was turned on and the AFS solution was circulated out of the vessel through the crystallizer and back to the vessel via the nozzle. The flow rate of the external slurry loop was 2.4 L·min$^{-1}$. In the curve of the 1$^{st}$ derivative of pressure, an obvious valley appeared when the external loop started. Meanwhile, a temperature peak and a big pressure drop appeared, indicating the start of $CO_2$ hydrate formation. The $CO_2$ uptake rose at the same time to 27.5 g, and it continued to grow gradually during the formation. An obvious increase also occurred in the charged capacity due to the latent heat exchange in hydrate formation.

After 2.0 h, the ultrasonic transducer on the crystallizer was turned on. It can be seen that after the ultrasonic transducer was switched on, the 1$^{st}$ derivative of pressure became scattered due to the vibration. However, the temperature curves, the pressure curve and the rate of charged capacity were unchanged. Therefore, it is believed that ultrasonic vibration does not affect the hydrate formation period once the formation has already started.

**7.2 Maximum valid chilled water temperature**

The stepwise method was used to determine the maximum chilled water temperature that could trigger the hydrate formation under the current pressure conditions (defined as the 'maximum valid chilled water temperature' in the present study). The maximum valid chilled water temperature could also correspond to the minimum supercooling degree of PCM.

The pressure was constant at 5.0 bar throughout the experiment. The chilled water temperature was first cooled down to 8.5$^0$C, which was higher than the maximum valid chilled water temperature at such pressure. As is shown in Figure 14, at 1.5 h after cooling, with no hydrate formation observed, the chilled water temperature was lowered by 0.5$^0$C. Sequentially, after another 1.5 h, there was still

ACCEPTED MANUSCRIPT

no formed solid or temperature peak or rise in charging rate observed. Therefore, the chilled water temperature was reduced by 0.5$^0$C again.

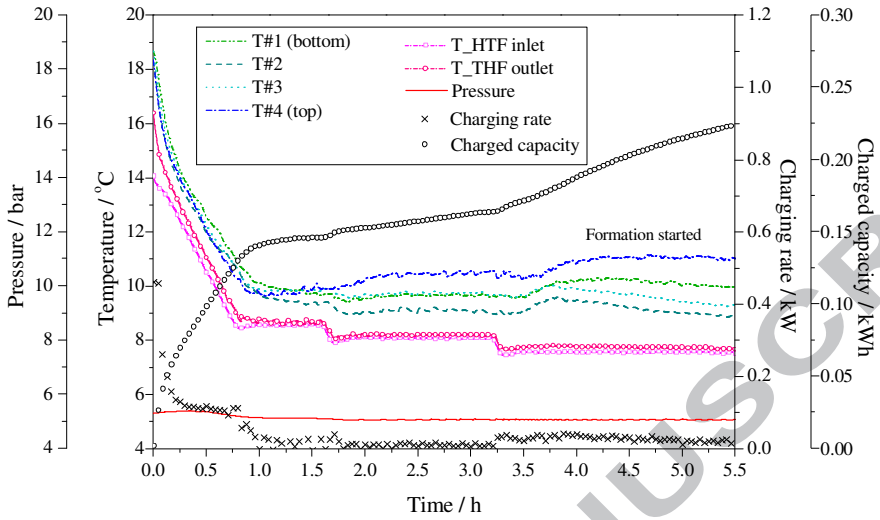


Figure 14 Temperature and charged capacity in the charge using the stepwise method

Immediately after the chilled water temperature reached 7.5$^0$C, a temperature peak occurred and the charging rate increased from 0.01 to 0.04 kW. The charged capacity started to grow rapidly. All these readings indicated that 7.5$^0$C chilled water triggered hydrate formation; thus it is considered to be the maximum valid chilled water temperature for the formation at 5.0 bar. The accuracy can be enhanced by repeating this method with smaller incremental temperature increases (e.g. 0.1$^0$C).

### 7.3 Influencing factors of the charging rate

#### 7.3.1 Chiller's set-point

In the practical operation of a cooling system, the higher the chiller's set-point, the higher the energy efficiency achieved. Therefore, it is important to know how the chilled water temperature can affect the charging performance of the CTES.

In these experiments, the outlet water temperature from the thermostatic bath was set at 5.0, 6.0 and 7.0$^0$C, respectively, and the chilled water flow rate was constant at 3.6 L·min$^{-1}$. The flow rate of the external slurry loop was also constant at 2.4 L·min$^{-1}$. The 'constant mass' mode was adopted and the initial pressure was 4.5 bar. The results are shown in Figure 15.

ACCEPTED MANUSCRIPT

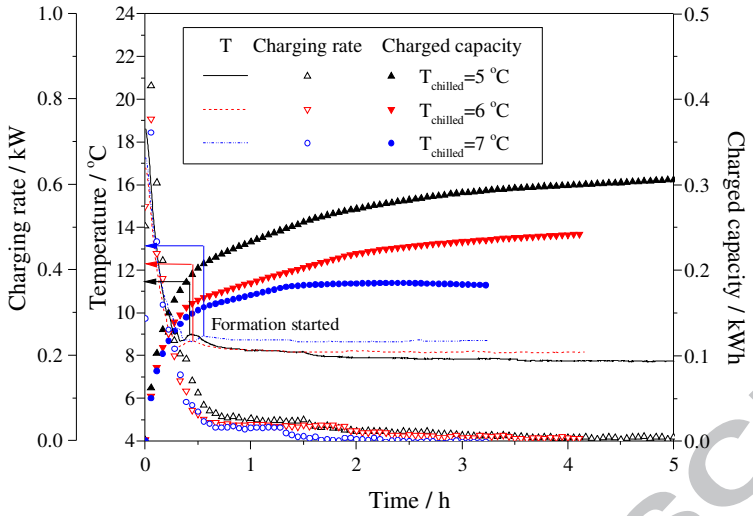


Figure 15 Effect of chiller's set-point on the charging rate

From the temperature curves, the induction times were 0.15, 0.19 and 0.21 h for 5.0, 6.0 and 7.0$^0$C chilled water, respectively. It is obvious that the charging rate was the highest for 5.0$^0$C chilled water followed by that for 6.0$^0$C chilled water. The charged capacity finally achieved 0.18, 0.24 and 0.31 kWh for 7.0, 6.0 and 5.0$^0$C chilled water. The discrepancy in the charged cooling capacity mainly resulted from the latent heat storage capacity by means of $CO_2$ hydrate formation. High driving force of subcooling (difference between the chilled water temperature and the equilibrium temperature of hydrate) greatly increased the charged capacity by enhancing hydrate formation. By comparison, the case of 7.0$^0$C chilled water resulted in poor charged cooling capacity due to the low subcooling – the hydrate formation finally ceased at 1.3 h with the charging rate dropping to 0.01 kW and the charged cooling capacity failing to increase any further. Different sensible heat transfer rates at various chilled water temperatures also accounted for a part of the discrepancy in the final charged capacity, but it is negligible compared to latent heat transfer. This trade-off between the charging temperature and charging capacity is an important operational constraint for the gas hydrate CTES.

### 7.3.2 External flow rate

The external slurry loop was found to be of significance to the hydrate formation, as deduced from Figure 13. This section describes the study of how the flow rate of the external loop could affect the charging rate of the CTES.

With the chilled water constant at 7.0$^0$C for all cases, the flow rate of the external loop was varied – 1.2, 1.8 and 2.4 L·min$^{-1}$. The 'constant mass' mode was adopted and the initial pressure was 4.5 bar. The results are shown in Figure 16.

ACCEPTED MANUSCRIPT

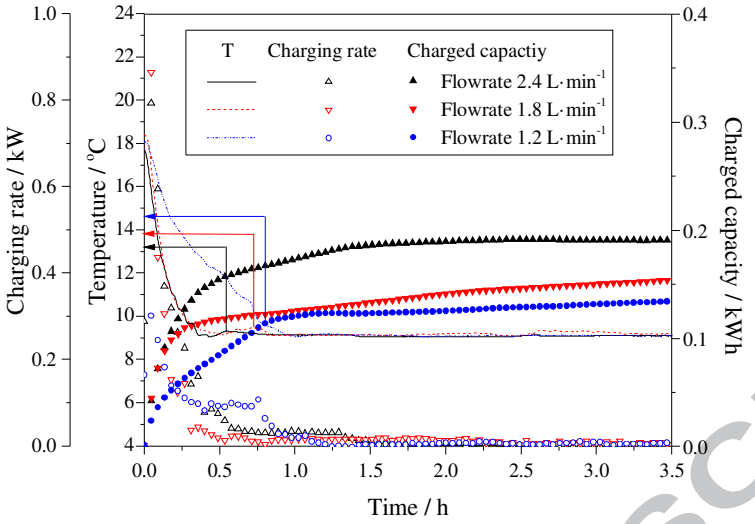


Figure 16 Effect of external flow rate on the charging rate

The induction time was 0.20 and 0.37 h, respectively, for the flow rate of 2.4 and 1.8 L·min$^{-1}$. This is attributed to the fact that, using a high flow rate the nozzle injected the circulated liquid back to the bulk of solution, and thus the convection heat transfer between the outer surface of the helical coil and the bulk of solution was enhanced; using 1.2 L·min$^{-1}$ flow rate, the convection heat transfer was weak; thus the sensible heat transfer period before hydrate formation was diminished. The charged capacity was finally 0.13, 0.15 and 0.19 kWh for 1.2, 1.8 and 2.4 L·min$^{-1}$. This indicates that the flow rate of the external loop played a significant role in the effective charge of the cold store, since it could improve both the convection heat transfer and the mass transfer between $CO_2$ gas and AFS solution greatly. When employing 1.2 L·min$^{-1}$ flow rate, the charging rate was found very low in the first 0.5 h and it increased rapidly between 0.5–1.0 h. This indicates that low flow rates are adverse to the incipient hydrate formation due to weak heat transfer.

There was an obvious difference between the charged capacity in the result for 2.4 L·min$^{-1}$ and that in Figure 13. This is owing to the different pressure conditions – 'constant mass' mode was used in both cases; however, the feed pressure was 5.5 bar in Figure 13 while it was 4.5 bar in Figure 16. This comparison reveals the effect of the overpressure driving force on the charged capacity.

### 7.3.3 Ultrasonic vibration

The effect of ultrasonic vibration on the charging process in Figure 13 shows that it does not affect the formation period if the hydrate formation has started. This test examines whether ultrasonic vibration affects the induction period before the formation starts. Two trials were carried out under the same conditions – a constant pressure of 5.0 bar and constant chilled water temperature of 7.0$^0$C.

ACCEPTED MANUSCRIPT

From the results shown in Figure 17, in the case without ultrasonic vibration, after the large sensible temperature decrease a lag appeared in the charged capacity, before it continued to increase (from 1.3 to 1.8 h). During this period, the charging rate decreased to 0. This lag was not found in the charged capacity of the case with ultrasonic vibration. The charged capacity of both cases was very close in the end. This reveals that the ultrasonic vibration may help to break the metastability and reduce the induction time, and thus accelerate the charging process; however, it does not show a major impact on the formation period and the charged capacity that a CTES can store.

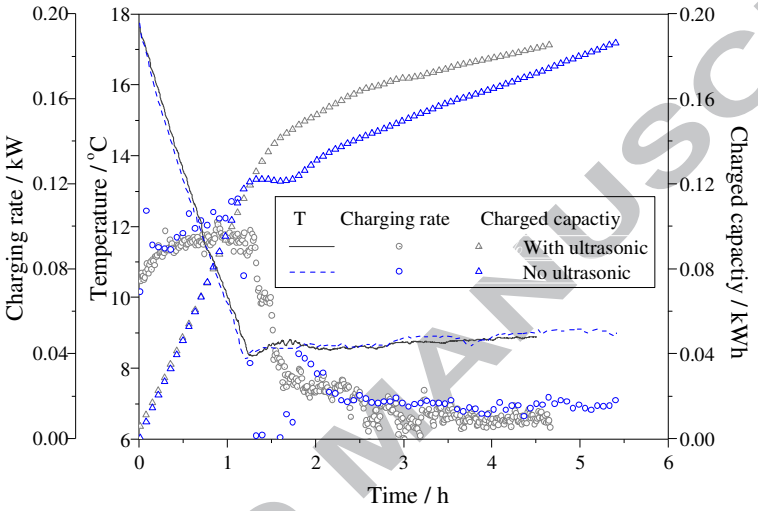


Figure 17 Effect of ultrasonic vibration on the charging rate

### 7.4 Charge control strategies

There are two control strategies of charging operation – constant mass and constant pressure. The trials are to investigate what charged cooling capacity can be achieved using different strategies. They were conducted at the same chilled water temperature of 7.0$^0$C. The pressure of 'constant mass' was initially 6.1 bar and it was finally decreased to 4.5 bar after the charging process; the pressure of 'constant pressure' was maintained at around 5.3 bar (the average pressure of the 'constant mass').

As shown in Figure 18, the charged capacity increased more slowly in the case of constant mass. The final charged capacity of the 'constant mass' case (0.24 kWh) was much smaller than that of the 'constant pressure' case (0.31 kWh). The reason for this discrepancy can be found in Figure 4. Adopting 'constant pressure' can make the required chilled water temperature higher than using 'constant mass'. This test was at the same chilled water temperature, which makes the subcooling driving force larger for the 'constant pressure' case than that of the 'constant mass' case. Hence, the charged capacity of the 'constant pressure' case was larger.

ACCEPTED MANUSCRIPT

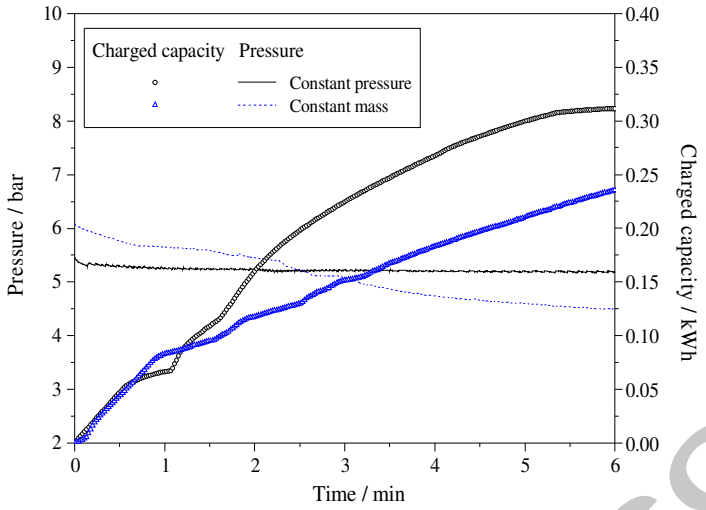


Figure 18 Pressure and charged capacity for 'constant mass' or 'constant pressure' mode

### 7.5 Repeatability of $CO_2$ hydrate formation

It was discussed previously that the formation data of gas hydrate usually has low repeatability. It imposes a big concern on the stability of the $CO_2$–AFS semi-clathrate in the repeated operations of a practical system. To study the formation repeatability, the charging-discharging process was repeated twenty times using the 'constant pressure' mode, and the formation temperature under experimental pressure of 5.0 bar was recorded. However, due to the error of the pressure control system these trials were conducted within the pressure range of 4.8–5.3 bar. There was limited ability to tightly control the gas delivery pressure, and this resulted in some scatter in the data.

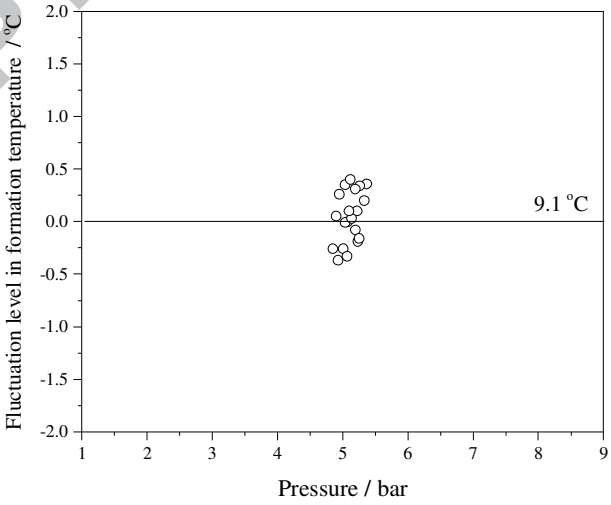


Figure 19 Formation temperature of $CO_2$-AFS semi-clathrate in 20 cycles of cold storage

ACCEPTED MANUSCRIPT

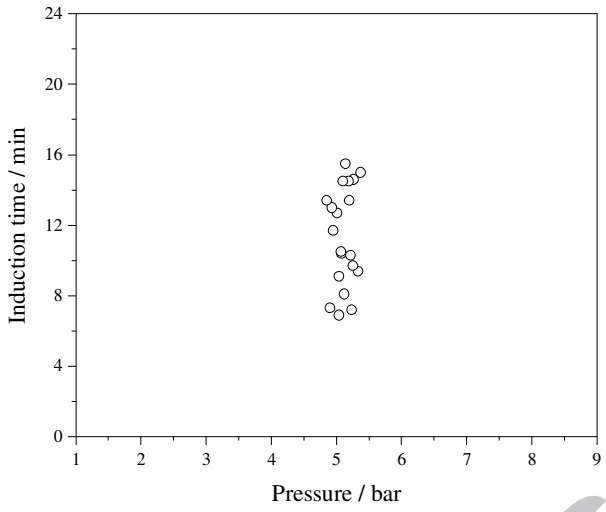


Figure 20 Induction time of $CO_2$–AFS semi-clathrate in 20 cycles of cold storage

Results from twenty experiments were plotted – the formation temperature is shown in Figure 19 and the induction time is shown in Figure 20. The average formation temperature measured was $9.1^0$C. The error in the measured formation temperatures were in a range of –0.4 to $0.4^0$C. Despite some scatter, the range of formation temperatures does not pose problems for the operation of a real gas hydrate CTES. The induction times measured were all below 15.5 min, which is acceptable for the charge of the CTES, but repeatability was poor.

## 8 Conclusions

CTES can aid in the efficient deployment of thermal energy whenever there is a mismatch between energy generation and use. Various subsets of CTES processes have been investigated and developed for building cooling systems. In this study, a lab-scale demonstration of cold storage system was built to investigate the performance of formation of $CO_2$ semi-clathrate hydrate in realistic CTES cooling system operating conditions.

(1) The effectiveness of charging the CTES was compared in three operation modes. It was found that for the experimental system, the hydrate formation could only proceed effectively when using the external loop with nozzle.

(2) Using the stepwise temperature reduction method, $7.5^0$C was found to be maximum valid chilled water temperature for the $CO_2$–AFS hydrate formation at constant pressure of 5.0 bar.

(3) Substantial subcooling can increase the storage capacity of the hydrate. Also, the external loop flow rate played a significant role in the effective charge of the CTES, since it could improve both

ACCEPTED MANUSCRIPT

the convection heat transfer and the mass transfer between $CO_2$ and water. Ultrasonic vibration can reduce the induction period; however, it had no obvious effect on the formation period.

(4) Using 'constant pressure' in the charge made the required chilled water temperature higher than when using 'constant mass'. This allows the chiller to operate more efficiently. Also, the charged capacity of using 'constant pressure' was greater than that of using 'constant mass'. It is suggested that the 'constant pressure' operation be adopted in practical cold storage systems.

(5) The CTES with 6.5 L AFS solution (containing 1.34 kg TBAB) is able to store 0.41 kWh cooling capacity if all TBAB is enclathrated. However, it was found that the storage capacity of the CTES was less than that. This reveals that the hydrate formation is not complete due to the lack of sufficient driving force or heat/mass transfer.

(6) 20 times of repeated experiments showed that the formation temperatures were stabile for the use in a real CTES; the induction times, although varied to some extent, were all short enough for practical operations.

The charging performance of $CO_2$ hydrate as a PCM is investigated by experiment in this study. It is obvious that the discharge process that releases cooling capacity to the users is also of importance for system evaluation. The discharging process of the same system and an explicit evaluation of the cold storage performance have been reported in another work [19].

ACCEPTED MANUSCRIPT

ACCEPTED MANUSCRIPT

**Reference**

[1] Tomorrow's energy today for cities and counties – keep it cool with thermal energy storage. U.S. Department of Energy 1995.

[2] A. Real, V. García, L. Domenech, J. Renau, N. Montés, F. Sánchez. Improvement of a heat pump based HVAC system with PCM thermal storage for cold accumulation and heat dissipation. Energy and Buildings 2014;83:108–116.

[3] Xiwen Cheng, Xiaoqiang Zhai, Ruzhu Wang. Thermal performance analysis of a packed bed cold storage unit using composite PCM capsules for high temperature solar cooling application. Applied Thermal Engineering 2016;100:247–255.

[4] A. Castell, M. Belusko, F. Bruno, L.F. Cabeza. Maximisation of heat transfer in a coil in tank PCM cold storage system. Applied Energy 2011;88:4120–4127.

[5] Christoph Zauner, Florian Hengstberger, Mark Etzel, Daniel Lager, Rene Hofmann, Heimo Walter. Experimental characterization and simulation of a fin-tube latent heat storage using high density polyethylene as PCM. Applied Energy 2016;179:237–246.

[6] Marcello De Falco, Mauro Capocelli, Alberto Giannattasio. Performance analysis of an innovative PCM-based device for cold storage in the civil air conditioning. Energy and Buildings 2016;122:1–10.

[7] Xiangjie Chen, Mark Worall, Siddig Omer, Yuehong Su, Saffa Riffat. Experimental investigation on PCM cold storage integrated with ejector cooling system. Applied Thermal Engineering 2014;63:419–427.

[8] Xiao-Yan Li, Qiao-Qiao Zhao, Dong-Qi Qu. Investigation on the dynamic characteristics of a direct contact thermal energy storage charging process for use in conventional air-conditioning systems. Applied Thermal Engineering 2015;91:172–180.

[9] Gabriele Comodi, Francesco Carducci, Balamurugan Nagarajan, Alessandro Romagnoli. Application of cold thermal energy storage (CTES) for building demand management in hot climates. Applied Thermal Engineering 2016;103:1186–1195.

[10] Yosr Allouche, Szabolcs Varga, Chiheb Bouden, et al. Experimental determination of the heat transfer and cold storage characteristics of a microencapsulated phase change material in a horizontal tank. Energy Convers Manage 2015;94:275–85.

ACCEPTED MANUSCRIPT

[11] X.J. Shi, P. Zhang. A comparative study of different methods for the generation of tetra-n-butyl ammonium bromide clathrate hydrate slurry in a cold storage air-conditioning system. Applied Energy 2013;112:1393–1402.

[12] Sloan, E., Koh, C. Clathrate hydrates of natural gases. Boca Raton, FL: CRC Press, 2008.

[13] Fournaison, L., Delahaye, A., Chatti, I., Petitet, J. $CO_2$ Hydrates in Refrigeration Processes. Industrial & Engineering Chemistry Research, 2004;43(20):6521–6526.

[14] Marinhas, S., Delahaye, A., Fournaison, L., Dalmazzone, D., Fürst, W., Petitet, J. Modelling of the available latent heat of a $CO_2$ hydrate slurry in an experimental loop applied to secondary refrigeration. Chemical Engineering and Processing: Process Intensification, 2006;45(3):184–192.

[15] H. Zhou, I.E.E. de Sera, C.A. Infante Ferreira. Modelling and experimental validation of a fluidized bed based CO2 hydrate cold storage system. Applied Energy 2015;158:433–445.

[16] Shin'ya Obara, Yoshinobu Kikuchi, Kyosuke Ishikawa, Masahito Kawai, Kashiwaya Yoshiaki. Development of a compound energy system for cold region houses using small-scale natural gas cogeneration and a gas hydrate battery. Energy 2015;85:280–295.

[17] C. Dorgan, J. Elleson. Design guide for cool thermal storage. Atlanta, GA: ASHRAE 1993;7–12.

[18] Xiaolin Wang, Mike Dennis. Phase equilibrium and formation behaviour of $CO_2$-TBAB semi-clathrate hydrate at low pressures for cold storage air conditioning applications. Chemical Engineering Science 2016;155:294–305.

[19] Xiaolin Wang, Mike Dennis. Thermal energy harvest in the discharge of $CO_2$ semi-clathrate hydrate in an emulated cold storage system. Applied Thermal Engineering 2017;124:725–733.

ACCEPTED MANUSCRIPT

ACCEPTED MANUSCRIPT

## Highlights

- We build an emulated cold storage system and employ a self-developed $CO_2$–AFS hydrate as PCM
- An external loop with a nozzle and an ultrasonic vibration is added to the system to improve hydrate formation
- 'Constant pressure' mode and 'constant mass' mode are compared concerning the ability to store cooling capacity
- We examine the influencing factors on the charging performance of the cold storage

ACCEPTED MANUSCRIPT